Editors' Suggestion | Featured in Physics

Realization of a Coherent and Efficient One-Dimensional Atom

Natasha Tomm,[1] Nadia O. Antoniadis,[1,*] Marcelo Janovitch,[1,†] Matteo Brunelli,[1] Rüdiger Schott,[2] Sascha R. Valentin,[2] Andreas D. Wieck,[2] Arne Ludwig,[2] Patrick P. Potts,[1] Alisa Javadi,[1,‡] and Richard J. Warburton[1]

[1]*Department of Physics, University of Basel, Klingelbergstrasse 82, CH-4056 Basel, Switzerland*
[2]*Lehrstuhl für Angewandte Festkörperphysik, Ruhr-Universität Bochum, D-44780 Bochum, Germany*

(Received 23 February 2024; accepted 8 July 2024; published 21 August 2024)

A quantum emitter interacting with photons in a single optical-mode constitutes a one-dimensional atom. A coherent and efficiently coupled one-dimensional atom provides a large nonlinearity, enabling photonic quantum gates. Achieving a high coupling efficiency (β factor) and low dephasing is challenging. Here, we use a semiconductor quantum dot in an open microcavity as an implementation of a one-dimensional atom. With a weak laser input, we achieve an extinction of 99.2% in transmission and a concomitant bunching in the photon statistics of $g^{(2)}(0) = 587$, showcasing the reflection of the single-photon component and the transmission of the multi-photon components of the coherent input. The tunable nature of the microcavity allows β to be adjusted and gives control over the photon statistics—from strong bunching to antibunching—and the phase of the transmitted photons. We obtain excellent agreement between experiment and theory by going beyond the single-mode Jaynes-Cummings model. Our results pave the way towards the creation of exotic photonic states and two-photon phase gates.

DOI: 10.1103/PhysRevLett.133.083602

Introduction—The ability to generate and manipulate correlated and entangled photonic states at the few-photon level is imperative for the advancement of photon-based quantum technologies. The realization of quantum photonic gates requires a highly nonlinear medium, i.e., a medium that enables a strong and controlled interaction of few photons [1–3]. A one-dimensional atom, a quantum emitter coupled to a single optical mode, is the ideal candidate to provide these functionalities [4]. Engineering a one-dimensional atom is challenging: the photon-emitter coupling efficiency, β, should be close to unity, and the emitter should be free of decoherence and noise. One approach is to employ an ensemble of atoms [5,6], which collectively behaves as a superatom, or a single emitter in a waveguide for which very high β factors have been achieved [7–10]. Cavity quantum electrodynamics provides an alternative route to a high β factor: a single emitter is embedded in a microcavity. This approach has been implemented with atoms [11–13], ions [14], molecules [15,16], and semiconductor quantum dots (QDs) [17–19].

Here, we embed a single QD in a one-sided microcavity, to create a one-dimensional atom following the original proposal of Ref. [20]. Important features are the exceptional coherence (low charge-noise [21], weak dephasing via phonons [22]) and the high β factor. We showcase the performance by measuring the transmission and reflection and their respective $g^{(2)}$ functions. In the ideal case, the emitter acts as a perfect mirror for single photons [23–25]. Our system shows an extinction of 99.2% of the transmitted light when probed with a low-power laser. Moreover, the transmitted state is highly bunched, $g^{(2)}(0) = 587$, a strong demonstration of the nonlinearity at the single-photon level.

The most striking results are the strong extinction and the high bunching of the transmitted state, both metrics for the nonlinearity, both much higher than in previous realizations [8,9,15,16,26]. Beyond this, first, we exploit the *in situ* tunability of the microcavity to tailor the photon statistics, transitioning from highly bunched to antibunched photonic states. Second, we present a full theoretical model. It includes two optical transitions and two cavity modes thereby going beyond the standard Jaynes-Cummings model. These details are crucial to describe the experimental results fully. Third, we exploit the Rice-Carmichael description of the cavity field [27] to obtain intuitive analytical expressions, which explain the main observations.

The experiment—The setup is depicted in Fig. 1(a). The cavity is an open microcavity [28] (highly miniaturized Fabry-Perot-type). The bottom mirror is a highly reflective (99.97%) semiconductor (AlAs/GaAs) DBR mirror. A layer of InAs QDs is embedded within an n-i-p diode structure [21]. The top mirror is a less reflective (99%)

*Contact author: nadia.antoniadis@unibas.ch
†Contact author: m.janovitch@unibas.ch
‡Present address: School of Electrical and Computer Engineering, Department of Physics and Astronomy, The University of Oklahoma, 110 West Boyd Street, Oklahoma 73019, USA.

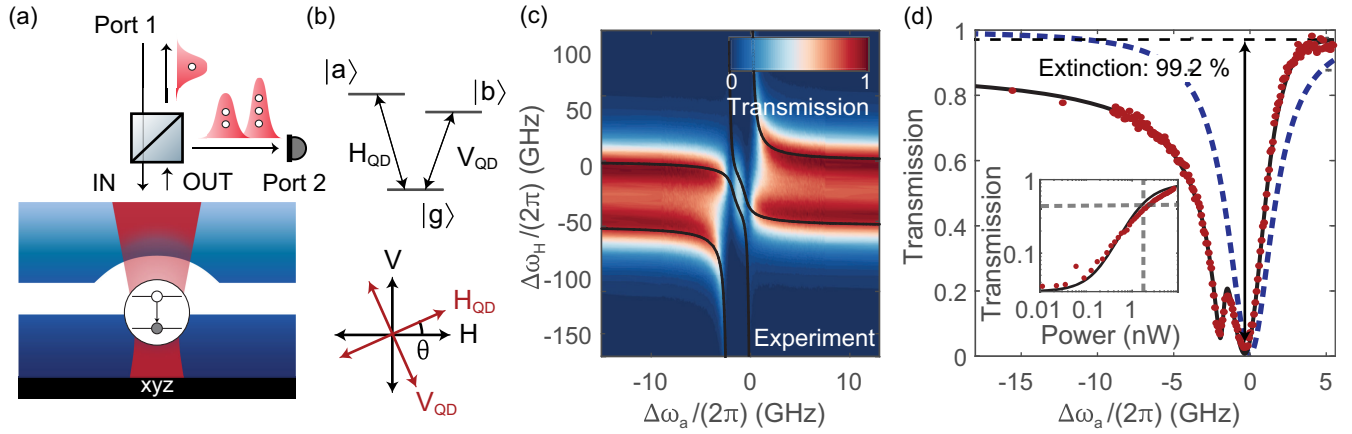

FIG. 1. A one-dimensional atom. (a) Experimental setup. Weak laser light impinges on a one-sided microcavity. The reflected light strikes a polarizing beam splitter. A half-wave plate sets an angle between the input and the axes of the cavity. The sketch shows the path for photons in transmission mode; the input is polarized at 45° relative to the cavity modes. At ideal QD-cavity coupling, single-photon components are reflected into port 1 and multiphoton components enter port 2. (b) Top: level structure of the neutral exciton. The two transitions have orthogonal linear polarizations. Bottom: polarization orientation of the horizontally (H) and vertically (V) polarized cavity modes and the QD transitions. (c) Transmission as a function of cavity detuning ($\Delta\omega_{\mathrm{H}}$) and QD detuning ($\Delta\omega_a$). Electrical tuning was employed keeping the laser frequency fixed: $\Delta\omega_{\mathrm{H}}$ is tuned via the piezo controlling z, the sample-top-mirror separation; $\Delta\omega_a$ is tuned via the voltage applied to the diode. Black lines indicate resonances between the laser frequency and the lowest transition frequencies of the Hamiltonian; see Ref. [31]. (d) Transmission for $\Delta\omega_{\mathrm{H}} = 0$. The transmission features two dips corresponding to the two QD transitions. The stronger transition shows an extinction of 99.2%. The black line is the full theoretical prediction showing excellent agreement with the data. The dashed blue line shows the JC model. The inset shows the power dependence of the transmission dip, with $P_{\mathrm{sat}} = 1.8$ nW (vertical dashed line).

dielectric DBR mirror (SiO_2/Ta_2O_5) on a silica substrate in which a microcrater is created by laser ablation. The sample and top mirror are the same as in Refs. [29,30]. The much higher transmittance of the top mirror makes the cavity one-sided: the top mirror of the cavity is the main access port for incoming and outgoing light [29]. The semiconductor is mounted on a set of xyz nanopositioners, allowing full control over the cavity length (z), also the QD lateral position relative to the cavity center (xy). A combination of a polarizing beam splitter and a half-wave plate gives full control over the polarization of the input and output states. The cavity mode is frequency split by $\delta_{\mathrm{cav}}/(2\pi) = (\omega_{\mathrm{H}} - \omega_{\mathrm{V}})/(2\pi) = 50$ GHz into two linearly and orthogonally polarized modes due to a small birefringence in the bottom mirror. We name these two polarizations H and V, with detunings $\Delta\omega_{\mathrm{H/V}} = \omega_{\mathrm{laser}} - \omega_{\mathrm{H/V}}$. The cavity modes have a loss rate $\kappa/(2\pi) = 28$ GHz.

We use a neutral exciton (X^0) in a QD. The QD was chosen according to two criteria: the exciton and cavity axes align reasonably well; the X^0 frequency lies in the intersection of the mirror stop bands. The X^0 has a V-level energy structure: one ground state $|g\rangle$ with two excited states $|a\rangle$ and $|b\rangle$ [Fig. 1(b)], with detunings $\Delta\omega_{a/b} = \omega_{\mathrm{laser}} - \omega_{a/b}$. The two QD transitions are linearly polarized, mutually orthogonal, and split in frequency by $\delta_{\mathrm{QD}}/(2\pi) = (\omega_a - \omega_b)/(2\pi) = 2.3$ GHz. The polarization axes of the QD lie at an angle of $\theta = 25.1°$ relative to the axis of the cavity [Fig. 1(b)]. Thus, the $\mathrm{H_{QD}}$ transition $|a\rangle \leftrightarrow |g\rangle$ couples more to the H- than to the V-polarized cavity mode, and vice versa for the $\mathrm{V_{QD}}$ transition $|b\rangle \leftrightarrow |g\rangle$. When optimally coupled to the cavity, the QD transitions have a Purcell-enhanced decay rate $\Gamma/(2\pi) = 1.65$ GHz (Purcell factor $F_{\mathrm{P}} = 11$), giving a maximum coupling efficiency $\beta = F_{\mathrm{P}}/(F_{\mathrm{P}} + 1) = 92\%$.

We use two experimental configurations termed "transmission" and "reflection." We focus first on the transmission mode: Light with polarization $P = (H + V)/\sqrt{2}$ is input from Port 1 and interacts with the QD-cavity system. The output is collected in Port 2, with polarization $M = (H - V)/\sqrt{2}$ [Fig. 1(a)]. We thus measure light transmitted from the P to the M polarization.

Strong extinction—The measured transmission as a function of QD detuning is shown in Fig. 1(d), illustrating an extinction of 99.2%, an immediate demonstration of the efficient QD-cavity coupling.

Some features can be understood with a JC model, obtained by setting $\theta = 0$ (ignoring the misalignment between the QD and cavity polarizations) and $|\delta_{\mathrm{cav}}|/\kappa \to \infty$ (large cavity-mode separation). In this case, only H-polarized light interacts with the QD cavity; V-polarized light is perfectly reflected. This model represents the canonical system, a two-level emitter coupled to a single cavity mode [20,27].

We consider first the case when the QD is far out of resonance [Fig. 1(c), far left or right]. When $\Delta\omega_{\mathrm{H}}$ is swept across zero, the phase of the reflected H-polarized light

winds around 2π while the V-polarized light remains unchanged. On resonance ($\Delta\omega_{\mathrm{H}} = 0$), the H-polarized light obtains a phase shift of π, turning P-polarized light into M-polarized light and resulting in a transmission close to unity. This explains the peaks in Fig. 1(c) when the laser is on resonance with one of the cavity modes (while the QD is out of resonance). Next, we consider sweeping the detuning of the QD $\Delta\omega_a$ at $\Delta\omega_{\mathrm{H}} = 0$ [Fig. 1(d)]. Crossing $\Delta\omega_a = 0$, the phase of the reflected H-polarized light again winds around 2π. This results in a dip in transmission; in the absence of dissipation, we expect perfect extinction ($T = 0$) on resonance ($\Delta\omega_a = \Delta\omega_{\mathrm{H}} = 0$). Dissipation reduces the transmission to $T = (1-\beta)^2$ [20,31].

Features of the transmission that are not captured by the JC model are the double-dip structure [Fig. 1(d)], and the shift of the maximal extinction to $\Delta\omega_a/(2\pi) \approx -0.31$ GHz. The double dip arises because in the presence of two QD transitions, sweeping $\Delta\omega_a$ results in the crossing of two resonances. The phase of the reflected H-polarized light then winds around 4π, resulting in two dips. Considering the full three-level system, the theory shows excellent agreement with experiment [Fig. 1(d)].

The maximum extinction is strongly dependent on the input power. With increasing laser power, the transmission dip disappears [inset, Fig. 1(d)]. This nonlinear response is a consequence of the saturation of the quantum emitter. We extract a saturation power of $P_{\mathrm{sat}} = 1.8$ nW [37], corresponding to a flux of 0.4 photons per QD lifetime.

Giant and tunable nonlinearity—We now demonstrate the ability of this cavity-QED setup to manipulate the statistics of the transmitted light. To this end, we consider the second-order correlation function $g^{(2)}(\tau)$, with τ the delay between detection events. We observe very strong bunching, $g^{(2)}(\tau = 0) = 587$ [Fig. 2(a)] for very low input power and an optimally coupled QD. To our knowledge, this is the largest photon-bunching due to a nonlinearity observed to date. Such a high bunching demands low dephasing, $\beta \simeq 1$, and high signal-to-laser-background ratio. Tuning β results in a change from strong bunching to antibunching [Fig. 2(b)], demonstrating wide control over the statistics of the transmitted light. In the experiment, β is tuned by laterally moving the QD relative to the cavity center.

The $g^{(2)}(\tau)$ function exhibiting giant bunching can be explained by the evolution of the M-polarized cavity field. In the bad-cavity, weak-drive limit, the cavity field is described by a pure quantum state at all times [27,31,32,38],

$$|\psi\rangle_\tau = |\alpha\rangle - i\sqrt{\frac{\Gamma}{2\kappa}}\langle\hat{\sigma}_{\mathrm{M}}\rangle_\tau \hat{a}_{\mathrm{M}}^\dagger|\alpha\rangle. \tag{1}$$

Here, $|\alpha\rangle$ denotes the coherent state describing the M mode in the absence of the QD. The second term describes the effect of the QD; $\hat{a}_{\mathrm{M}}^\dagger$ denotes the creation operator of the M mode, and $\hat{\sigma}_{\mathrm{M}}$ the QD transition coupled to the M polarization. Equation (1) provides the correct averages for any normal-ordered observable to leading order in the external drive. We refer to this state as the Rice-Carmichael (RC) state [27]. The $g^{(2)}$ function may then be understood as follows. Detecting a photon alters the field in the cavity, which then regresses to its steady state. The time-dependent average field gives $g^{(2)}(\tau) = |\langle\hat{a}_{\mathrm{M}}\rangle_\tau/\langle\hat{a}_{\mathrm{M}}\rangle_\infty|^2$, where the average is relative to $|\psi\rangle_\tau$ [27,31]. Thus, $g^{(2)}(\tau)$ larger (smaller) than 1 is observed whenever the average field is stronger (weaker) than in the steady state.

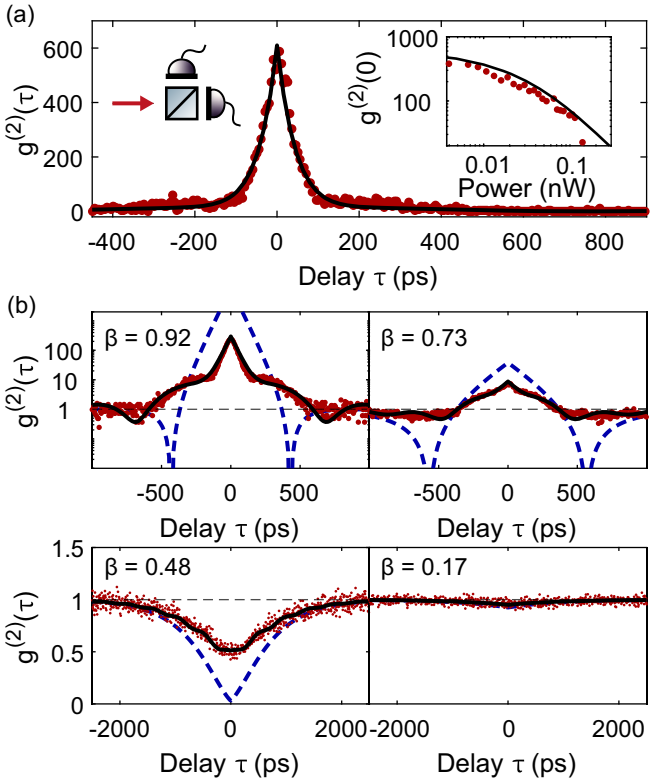

FIG. 2. Intensity correlations. (a) $g^{(2)}(\tau)$ of the transmitted light for $\Delta\omega_{\mathrm{H}} = 0$ and $\Delta\omega_a = -0.14$ GHz. The QD is positioned in the center of the cavity ($\beta = 0.92$). The input power is 0.3 pW corresponding to 0.000 67 photons per lifetime. The bin size is 5 ps, integration time 1 h; at large τ, signal on average 0.24 counts-per-bin. The single-photon detector has efficiency 80%, dark-count rate 100 Hz, and total timing jitter 50 ps. A bunching of 587 highlights the strong nonlinearity of the system. Inset shows $g^{(2)}(0)$ as a function of laser power, the black lines the theoretical model. (b) $g^{(2)}(\tau)$ for different QD positions, i.e., different β factors, for $\Delta\omega_{\mathrm{H}} = 0$ and $\Delta\omega_a/(2\pi) = -0.14$ GHz. Input power 17 pW, bin size and integration time as in (a); average counts-per-bin 8.2, 70, 414, 1700 for $\beta = 0.92$, 0.73, 0.48, and 0.17, respectively. Bunching turns into antibunching at $\beta \simeq 0.5$, and disappears for $\beta \to 0$. The full model (solid black line) is compared to the JC model (dashed blue line).

To explain the key aspects, we consider the RC state for the JC model. In this case, we find

$$\frac{\langle\hat{a}_{\mathrm{M}}\rangle_\tau}{\langle\hat{a}_{\mathrm{M}}\rangle_\infty} = 1 - \frac{\beta^2}{(1-\beta)^2} e^{-\frac{\gamma\tau}{2(1-\beta)}}, \tag{2}$$

where $\gamma = 2\Gamma/F_P$ denotes the dissipation rate of the QD. This shows that the photon statistics can be modified by tuning β. At $\beta \simeq 0$ the cavity field remains close to a coherent state while for $\beta \simeq 1$, the contribution to Eq. (2) stemming from the QD yields an amplified number of photons.

The transition from bunching to antibunching [Fig. 2(b)] may qualitatively be understood by considering the steady state in the Fock basis $\langle n|\psi\rangle_\infty = \alpha^n(1-\beta n)/\sqrt{n!}$. At $\beta = 1$ the single-photon component in the cavity vanishes and is thus perfectly reflected [sketch Fig. 1(a)]. Crucially, multiphoton components are present in the cavity, leading to giant bunching in the transmitted light. In particular, $|\langle 2|\psi\rangle_\infty|$ remains unchanged. In contrast, for $\beta = 1/2$, the two-photon component in the cavity vanishes, yielding perfect antibunching $g^{(2)}(0) = 0$. Similarly, tuning $\beta = 1/n$ allows the n-photon component to be suppressed.

Equation (2) implies that the average field in the cavity changes sign upon photodetection if $\beta > 1/2$. When the field subsequently crosses zero, $g^{(2)}$ vanishes [Fig. 2(b)].

Features not captured by the JC model include the shoulders in Fig. 2(b), which are related to the cavity and QD splittings, $\delta_{\mathrm{QD/cav}} \neq 0$. Furthermore, the antibunching is limited by the cavity-mode splitting $\delta_{\mathrm{cav}} \neq 0$ and the polarizations' misalignment, $\theta \neq 0$, such that $g^{(2)}(0) \simeq 0.5$ at $\beta \simeq 0.5$. Our full model shows excellent agreement with these features.

Photons are correlated in time—We now turn to the reflection mode experiment [39,40]. In this case, the cavity is driven by H-polarized light and the reflected light in the same polarization is measured. A 99:1 beam-splitter separates the input light from the output. Figure 3(a) shows the reflected signal $R_{\leftarrow}$. Because of the coupling to the QD, photons either dissipate or change polarization, reducing the reflection. Interestingly, the less-coupled QD transition results in a stronger reduction of the reflection [upper panel, Fig. 3(a)]. This is explained by the JC model, obtained for $\theta = 0$ in the reflection mode. Specifically, for $\Delta\omega_{\mathrm{H}} = \Delta\omega_a = 0$, $R_{\leftarrow} = (1-2\beta)^2$; then, for $\beta = 0.92$, we have a small dip in the reflection [blue line, Fig. 3(a)]. The less-coupled transition results in a pronounced dip: the reduced coupling is equivalent to a smaller β.

Turning to $g^{(2)}_{\leftarrow}(\tau)$, Fig. 3(b), we find a peak at zero delay $g^{(2)}_{\leftarrow}(0) = 7.3$, followed by a dip $g^{(2)}_{\leftarrow}(133\ \mathrm{ps}) = 0.25$. Photons are thus correlated at short delays and anticorrelated at longer delays. Thus, it is much more likely to observe them close to each other. This is consistent with the formation of bound states: photons are pulled together in time, forming a highly correlated state [30,41]. A similar effect is also predicted in the transmission mode [Fig. 2(b)], but there it lies below the noise floor due to the small transmission. The intensity correlations in the reflection mode can be described using an RC state: $g^{(2)}_{\leftarrow}(\tau) = |\langle\hat{b}_{\mathrm{H}}\rangle_\tau/\langle\hat{b}_{\mathrm{H}}\rangle_\infty|^2$, where the averages are computed from

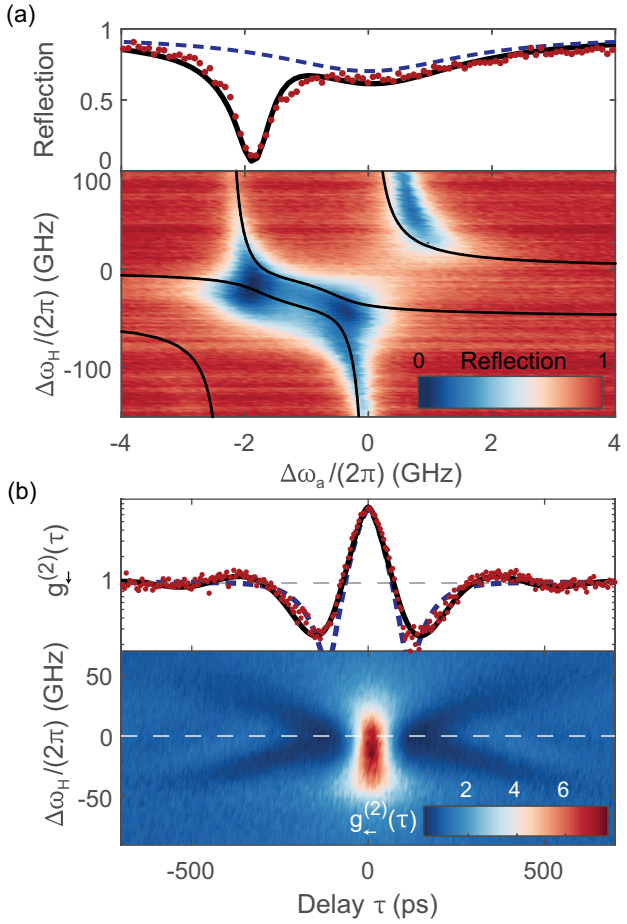

FIG. 3. Reflection mode (a) Top: Reflection as a function of QD detuning for $\Delta\omega_{\mathrm{H}} = 0$ and a power well below saturation. The weakly coupled QD transition results in a much deeper dip than the strongly coupled transition. Bottom: Reflection as a function of QD and cavity detuning. The black lines show the resonances between the laser frequency and the lowest transition frequencies of the Hamiltonian, see Ref. [31]. (b) Top: $g^{(2)}(\tau)$ at $\Delta\omega_{\mathrm{H}} = 0$, $\Delta\omega_a/(2\pi) = -0.14$ GHz. Correlation followed by anticorrelation is observed. Bottom: $g^{(2)}(\tau)$ versus $\Delta\omega_{\mathrm{H}}$. The dashed line marks the cut through, $\Delta\omega_{\mathrm{H}} = 0$. In the top panels, the full theoretical model (solid black line) is compared to the JC model (dashed blue line).

the RC state, and $\hat{b}_{\mathrm{H}}$ describes the cavity field displaced by the light that is directly reflected. The JC model again allows the qualitative features of the data to be understood. For $\Delta\omega_{\mathrm{H}} = \Delta\omega_a = 0$,

$$\frac{\langle\hat{b}_{\mathrm{H}}\rangle_\tau}{\langle\hat{b}_{\mathrm{H}}\rangle_\infty} = 1 - \frac{(2\beta)^2}{(1-2\beta)^2} e^{-\frac{\gamma\tau}{2(1-\beta)}}. \tag{3}$$

The field changes sign upon detecting a photon if $\beta > 1/4$. When regressing to the steady state, we must have $\langle\hat{b}_{\mathrm{H}}\rangle = 0$, yielding a vanishing $g^{(2)}_{\leftarrow}$ and explaining the anticorrelation at finite delays [31].

Conclusion and outlook—We have established efficient and coherent coupling between a QD and a microcavity. As a result, the QD behaves radically differently depending on the number of photons. This leads to a huge bunching, as only multiphoton states are transmitted. We find excellent agreement between experiment and theory by going beyond the single-mode JC model and including two QD transitions and two cavity modes in our model. The connection between the RC state and the $g^{(2)}$ suggests an intuitive understanding of photon statistics through the field's phase space.

The observed photon-number discriminating interaction enables photon-photon interactions at the single-photon limit and may find application in creating photonic bound states [30,42,43] and exotic photonic states [6], in establishing direction-dependent phase-shifts [39], and in studying many-body phenomena [44] in a controllable setting. The overall transmission of the setup, from the input fiber to the output fiber, is high, about 50% [29]. A promising avenue is to mimic the interaction between photons and multiple quantum emitters in series, e.g., via time-delayed feedback. This allows the generation of exotic bound states involving many photons [41]. Furthermore, this system may find application as a photon sorter [45–48] or a photon-photon quantum gate [49,50].

Acknowledgments—We thank Mark R. Hogg, Gabriel T. Landi, and Aaron Daniel for stimulating discussions. We acknowledge financial support from Horizon-2020 FET-Open Project QLUSTER, Swiss National Science Foundation Project No. 200020_204069, Eccellenza Professorial Fellowship PCEFP2_194268, and NCCR QSIT. A. J. acknowledges support from the European Union's Horizon 2020 Research and Innovation Programme under Marie Skłodowska-Curie Grant Agreement No. 840453 (HiFig). S. R. V., R. S., A. L., and A. D. W. acknowledge support from DFH/UFA CDFA05-06, DFG TRR160, DFG Project No. 383065199, and BMBF-QR.X Project No. 16KISQ009.

N. T., N. O. A., and M. J. contributed equally to this work.

[1] D. E. Chang, V. Vuletić, and M. D. Lukin, Quantum nonlinear optics—photon by photon, Nat. Photonics **8**, 685 (2014).

[2] M. J. Hartmann, Quantum simulation with interacting photons, J. Opt. **18**, 104005 (2016).

[3] D. E. Chang, J. S. Douglas, A. González-Tudela, C.-L. Hung, and H. J. Kimble, Colloquium: Quantum matter built from nanoscopic lattices of atoms and photons, Rev. Mod. Phys. **90**, 031002 (2018).

[4] J.-T. Shen and S. Fan, Strongly correlated multiparticle transport in one dimension through a quantum impurity, Phys. Rev. A **76**, 062709 (2007).

[5] H. L. Sørensen, J.-B. Béguin, K. W. Kluge, I. Iakoupov, A. S. Sørensen, J. H. Müller, E. S. Polzik, and J. Appel, Coherent backscattering of light off one-dimensional atomic strings, Phys. Rev. Lett. **117**, 133604 (2016).

[6] A. S. Prasad, J. Hinney, S. Mahmoodian, K. Hammerer, S. Rind, P. Schneeweiss, A. S. Sørensen, J. Volz, and A. Rauschenbeutel, Correlating photons using the collective nonlinear response of atoms weakly coupled to an optical mode, Nat. Photonics **14**, 719 (2020).

[7] M. Arcari, I. Söllner, A. Javadi, S. Lindskov Hansen, S. Mahmoodian, J. Liu, H. Thyrrestrup, E. H. Lee, J. D. Song, S. Stobbe, and P. Lodahl, Near-unity coupling efficiency of a quantum emitter to a photonic crystal waveguide, Phys. Rev. Lett. **113**, 093603 (2014).

[8] D. Hallett, A. P. Foster, D. L. Hurst, B. Royall, P. Kok, E. Clarke, I. E. Itskevich, A. M. Fox, M. S. Skolnick, and L. R. Wilson, Electrical control of nonlinear quantum optics in a nano-photonic waveguide, Optica **5**, 644 (2018).

[9] H. Le Jeannic, T. Ramos, S. F. Simonsen, T. Pregnolato, Z. Liu, R. Schott, A. D. Wieck, A. Ludwig, N. Rotenberg, J. J. García-Ripoll, and P. Lodahl, Experimental reconstruction of the few-photon nonlinear scattering matrix from a single quantum dot in a nanophotonic waveguide, Phys. Rev. Lett. **126**, 023603 (2021).

[10] H. Le Jeannic, A. Tiranov, J. Carolan, T. Ramos, Y. Wang, M. H. Appel, S. Scholz, A. D. Wieck, A. Ludwig, N. Rotenberg, L. Midolo, J. J. García-Ripoll, A. S. Sørensen, and P. Lodahl, Dynamical photon-photon interaction mediated by a quantum emitter, Nat. Phys. **18**, 1191 (2022).

[11] A. Goban, C.-L. Hung, S.-P. Yu, J. D. Hood, J. A. Muniz, J. H. Lee, M. J. Martin, A. C. McClung, K. S. Choi, D. E. Chang, O. Painter, and H. J. Kimble, Atom–light interactions in photonic crystals, Nat. Commun. **5**, 3808 (2014).

[12] T. G. Tiecke, J. D. Thompson, N. P. de Leon, L. R. Liu, V. Vuletić, and M. Lukin, Nanophotonic quantum phase switch with a single atom, Nature (London) **508**, 241 (2014).

[13] X. Luan, J.-B. Béguin, A. P. Burgers, Z. Qin, S.-P. Yu, and H. J. Kimble, The integration of photonic crystal waveguides with atom arrays in optical tweezers, Adv. Quantum Technol. **3**, 2000008 (2020).

[14] H. Takahashi, E. Kassa, C. Christoforou, and M. Keller, Strong coupling of a single ion to an optical cavity, Phys. Rev. Lett. **124**, 013602 (2020).

[15] D. Wang, H. Kelkar, D. Martin-Cano, D. Rattenbacher, A. Shkarin, T. Utikal, S. Götzinger, and V. Sandoghdar, Turning a molecule into a coherent two-level quantum system, Nat. Phys. **15**, 483 (2019).

[16] A. Pscherer, M. Meierhofer, D. Wang, H. Kelkar, D. Martín-Cano, T. Utikal, S. Götzinger, and V. Sandoghdar, Single-molecule vacuum Rabi splitting: Four-wave mixing and optical switching at the single-photon level, Phys. Rev. Lett. **127**, 133603 (2021).

[17] M. T. Rakher, N. G. Stoltz, L. A. Coldren, P. M. Petroff, and D. Bouwmeester, Externally mode-matched cavity quantum electrodynamics with charge-tunable quantum dots, Phys. Rev. Lett. **102**, 097403 (2009).

[18] L. De Santis, C. Antón, B. Reznychenko, N. Somaschi, G. Coppola, J. Senellart, C. Gómez, A. Lemaître, I. Sagnes, A. G. White, L. Lanco, A. Auffèves, and P. Senellart,

A solid-state single-photon filter, Nat. Nanotechnol. **12**, 663 (2017).
[19] D. Najer, I. Söllner, P. Sekatski, V. Dolique, M. C. Löbl, D. Riedel, R. Schott, S. Starosielec, S. R. Valentin, A. D. Wieck, N. Sangouard, A. Ludwig, and R. J. Warburton, A gated quantum dot strongly coupled to an optical microcavity, Nature (London) **575**, 622 (2019).
[20] A. Auffèves-Garnier, C. Simon, J.-M. Gérard, and J.-P. Poizat, Giant optical nonlinearity induced by a single two-level system interacting with a cavity in the Purcell regime, Phys. Rev. A **75**, 053823 (2007).
[21] A. V. Kuhlmann, J. Houel, A. Ludwig, L. Greuter, D. Reuter, A. D. Wieck, M. Poggio, and R. J. Warburton, Charge noise and spin noise in a semiconductor quantum device, Nat. Phys. **9**, 570 (2013).
[22] J. Iles-Smith, D. P. S. McCutcheon, A. Nazir, and J. Mork, Phonon scattering inhibits simultaneous near-unity efficiency and indistinguishability in semiconductor single-photon sources, Nat. Photonics **11**, 521 (2017).
[23] J. T. Shen and S. Fan, Coherent photon transport from spontaneous emission in one-dimensional waveguides, Opt. Lett. **30**, 2001 (2005).
[24] J.-T. Shen and S. Fan, Strongly correlated two-photon transport in a one-dimensional waveguide coupled to a two-level system, Phys. Rev. Lett. **98**, 153003 (2007).
[25] D. E. Chang, A. S. Sorensen, E. A. Demler, and M. D. Lukin, A single-photon transistor using nanoscale surface plasmons, Nat. Phys. **3**, 807 (2007).
[26] A. Javadi, I. Söllner, M. Arcari, S. L. Hansen, L. Midolo, S. Mahmoodian, G. Kiršanskė, T. Pregnolato, E. Lee, J. Song, S. Stobbe, and P. Lodahl, Single-photon non-linear optics with a quantum dot in a waveguide, Nat. Commun. **6**, 8655 (2015).
[27] P. R. Rice and H. J. Carmichael, Single-atom cavity-enhanced absorption. I. Photon statistics in the bad-cavity limit, IEEE J. Quantum Electron. **24**, 1351 (1988).
[28] R. J. Barbour, P. A. Dalgarno, A. Curran, K. M. Nowak, H. J. Baker, D. R. Hall, N. G. Stoltz, P. M. Petroff, and R. J. Warburton, A tunable microcavity, J. Appl. Phys. **110**, 053107 (2011).
[29] N. Tomm, A. Javadi, N. O. Antoniadis, D. Najer, M. C. Löbl, A. R. Korsch, R. Schott, S. R. Valentin, A. D. Wieck, A. Ludwig, and R. J. Warburton, A bright and fast source of coherent single photons, Nat. Nanotechnol. **16**, 399 (2021).
[30] N. Tomm, S. Mahmoodian, N. O. Antoniadis, R. Schott, S. R. Valentin, A. D. Wieck, A. Ludwig, A. Javadi, and R. J. Warburton, Direct observation of photon bound states using a single artificial atom, Nat. Phys. **19**, 857 (2023).
[31] See Supplemental Material at http://link.aps.org/supplemental/10.1103/PhysRevLett.133.083602 for the full theoretical description used in the text together with the connection of the simplified scenarios and the construction of the reduced cavity states (Rice-Carmichael states). We also include a table with all the parameters used in each figure in the text for the theory curves. We include Refs. [27,32–36].
[32] H. Carmichael, *Statistical Methods in Quantum Optics 2* (Springer Berlin Heidelberg, Berlin, Heidelberg, 2008).
[33] C. W. Gardiner and M. J. Collett, Input and output in damped quantum systems: Quantum stochastic differential equations and the master equation, Phys. Rev. A **31**, 3761 (1985).
[34] A. Auffèves-Garnier, C. Simon, J.-M. Gérard, and J.-P. Poizat, Giant optical nonlinearity induced by a single two-level system interacting with a cavity in the Purcell regime, Phys. Rev. A **75**, 053823 (2007).
[35] H.-P. Breuer and F. Petruccione, *The Theory of Open Quantum Systems* (Oxford University Press, New York, 2002).
[36] D. F. Walls and G. J. Milburn, *Quantum Optics*, 2nd ed. (Springer Verlag, Berlin, 2008).
[37] The theory predicts $P_{\mathrm{sat}} = 1.5$ nW; the mismatch is attributed to losses [31].
[38] H. J. Carmichael, R. J. Brecha, M. G. Raizen, H. J. Kimble, and P. R. Rice, Subnatural linewidth averaging for coupled atomic and cavity-mode oscillators, Phys. Rev. A **40**, 5516 (1989).
[39] P. Lodahl, S. Mahmoodian, S. Stobbe, A. Rauschenbeutel, P. Schneeweiss, J. Volz, H. Pichler, and P. Zoller, Chiral quantum optics, Nature (London) **541**, 473 (2017).
[40] N. O. Antoniadis, N. Tomm, T. Jakubczyk, R. Schott, S. R. Valentin, A. D. Wieck, A. Ludwig, R. J. Warburton, and A. Javadi, A chiral one-dimensional atom using a quantum dot in an open microcavity, npj Quantum Inf. **8**, 27 (2022).
[41] S. Mahmoodian, G. Calajó, D. E. Chang, K. Hammerer, and A. S. Sørensen, Dynamics of many-body photon bound states in chiral waveguide QED, Phys. Rev. X **10**, 031011 (2020).
[42] N. Stiesdal, J. Kumlin, K. Kleinbeck, P. Lunt, C. Braun, A. Paris-Mandoki, C. Tresp, H. P. Büchler, and S. Hofferberth, Observation of three-body correlations for photons coupled to a Rydberg superatom, Phys. Rev. Lett. **121**, 103601 (2018).
[43] Q.-Y. Liang, A. V. Venkatramani, S. H. Cantu, T. L. Nicholson, M. J. Gullans, A. V. Gorshkov, J. D. Thompson, C. Chin, M. D. Lukin, and V. Vuletić, Observation of three-photon bound states in a quantum nonlinear medium, Science **359**, 783 (2018).
[44] C. Noh and D. G. Angelakis, Quantum simulations and many-body physics with light, Rep. Prog. Phys. **80**, 016401 (2016).
[45] T. C. Ralph, I. Söllner, S. Mahmoodian, A. G. White, and P. Lodahl, Photon sorting, efficient Bell measurements, and a deterministic controlled-Z gate using a passive two-level nonlinearity, Phys. Rev. Lett. **114**, 173603 (2015).
[46] F. Yang, M. M. Lund, T. Pohl, P. Lodahl, and K. Mølmer, Deterministic photon sorting in waveguide QED systems, Phys. Rev. Lett. **128**, 213603 (2022).
[47] D. Witthaut, M. D. Lukin, and A. S. Sørensen, Photon sorters and QND detectors using single photon emitters, Europhys. Lett. **97**, 50007 (2012).
[48] I. Shomroni, S. Rosenblum, Y. Lovsky, O. Bechler, G. Guendelman, and B. Dayan, All-optical routing of single photons by a one-atom switch controlled by a single photon, Science **345**, 903 (2014).
[49] Z. Chen, Y. Zhou, J.-T. Shen, P.-C. Ku, and D. Steel, Two-photon controlled-phase gates enabled by photonic dimers, Phys. Rev. A **103**, 052610 (2021).
[50] D. J. Brod and J. Combes, Passive CPHASE gate via cross-Kerr nonlinearities, Phys. Rev. Lett. **117**, 080502 (2016).